



# Global ionospheric modeling based on multi-GNSS, satellite altimetry, and Formosat-3/COSMIC data

Yibin Yao<sup>1,2,3</sup> · Lei Liu<sup>1</sup> · Jian Kong<sup>4</sup> · Changzhi Zhai<sup>1</sup>

Received: 12 September 2017 / Accepted: 25 July 2018  
© Springer-Verlag GmbH Germany, part of Springer Nature 2018

## Abstract

Ionosphere total electron content (TEC) from global ionospheric maps (GIM) is widely applied in both ionospheric delay correction and research on space weather monitoring. Global ionospheric modeling based on multisource data is an effective method to improve conventional GIM accuracy and reliability. In this study, a global ionospheric model is constructed from multi-GNSS (here, GPS/GLONASS/BDS), satellite altimetry and Formosat-3/COSMIC (F3/C) observations using a spherical harmonic (SH) function. The results show that compared to the conventional GIM derived from GPS/GLONASS data, the combined GIM performance from multisource data improves significantly; the RMS versus external data decreases from [2, 5] to [2, 3] TECU, and the BIAS decreases from [− 3, 1] to [− 1, 1] TECU. Specifically, BDS observations improve the IPP distributions, especially over the region of Australia; compared with GPS-based ionospheric TEC. Our calculated GIM with BDS data has better performance than that without BDS data. By combining JASON 2 and GPS/GLONASS data, the residual distribution is more concentrated, and the RMS is improved effectively in mid-high latitudes of the southern hemisphere and in the equatorial region. F3/C TEC also exhibits relatively minor improvements on GIM; the standard deviation reduces from 2.89 to 1.92 TECU, and the BIAS regarding extra F3/C data decreases from − 2.02 to − 1.71 TECU.

**Keywords** Global ionospheric maps (GIM) · Total electron content (TEC) · Multi-GNSS · Satellite altimetry · Formosat-3/COSMIC (F3/C) occultation

## Introduction

With the rapid development of global navigation satellite system (GNSS) technology, GNSS-based global ionospheric monitoring and modeling have become popular subject of research (Yuan et al. 2008; Li et al. 2012; Alizadeh et al. 2011; Chen et al. 2017; Roma-Dollase et al. 2017). Currently, the International GNSS Service (IGS) ionospheric

working group consists of seven Ionospheric Associate Analysis Centers (IAACs), namely, the Centre for Orbit Determination in Europe (CODE), Jet Propulsion Laboratory (JPL), European Space Agency (ESA), Polytechnic University of Catalonia (UPC), Natural Resources Canada (NRCan/EMR), Chinese Academy of Sciences (CAS/IGG), and Wuhan University (WHU). Among these IAACs, the approaches for providing global ionosphere products are different. The GIM from CODE, ESA, NRCan/EMR, and WHU is developed using a  $15 \times 15$  spherical harmonic function model, with some differences in their processing details (Schaer 1999; Feltens 2007; Zhang et al. 2013). JPL's technique is based on a linear composition of bi-cubic spline interpolation within 1280 spherical triangular tiles that tessellate the ionosphere, corresponding to 642 vertices (Manucci et al. 1998). UPC independently computes the TEC with a multi-layer tomographic model and an interpolation scheme (Hernández-Pajares et al. 1999; Orús et al. 2003). The CAS approach for GIM relies on integrating the spherical harmonic and the generalized trigonometric series functions on global and local scales, respectively (Li et al. 2015).

✉ Yibin Yao  
ybyao@whu.edu.cn

✉ Lei Liu  
leiliu@whu.edu.cn

<sup>1</sup> School of Geodesy and Geomatics, Wuhan University, Wuhan, China

<sup>2</sup> Key Laboratory of Geospace Environment and Geodesy, Ministry of Education, Wuhan University, Wuhan, China

<sup>3</sup> Collaborative Innovation Center for Geospatial Technology, Wuhan, China

<sup>4</sup> Chinese Antarctic Center of Surveying and Mapping, Wuhan University, Wuhan, China

The final GIM from IGS is obtained from the independently computed ones by different IAACs which are combined with the corresponding weights (Hernández-Pajares et al. 2009).

Conventional ionospheric modeling is usually based on GPS measurements or GPS/GLONASS measurements; it should be noted that with the development of multi-GNSS, especially the BeiDou system (BDS), more GNSS observations will be available, helping to increase the spatial coverage of IPPs and improve ionospheric modeling accuracy. Tang et al. (2014) focused on the performance of ionosphere monitoring using the measurements from a BeiDou CORS network. Zhang et al. (2015) also analyzed the influence of BeiDou on ionospheric modeling and found that the GPS/BDS dual system could improve both the ionospheric model over the China sector and the accuracy of differential code bias (DCB) determination. Xue et al. (2016) constructed a global ionospheric model based on BDS/GPS dual-system observations and provided a detailed analysis of the stability of the resulting BDS DCB estimates.

However, the IPPs from multi-GNSS measurements mainly improve the spatial distributions over continental regions, whereas few effective GNSS measurements are available over oceans. This results in a limited accuracy of GIMs in ocean areas and some other areas where GNSS sites are uneven and sparse. To improve the accuracy of the GIM, especially over ocean areas, some studies have been done based on multisource data in recent years. For example, Dettmering et al. (2011) introduced a method to compute the regional ionospheric model based on the International Reference Ionosphere (IRI), GPS observations, radio occultation data and radar altimetry measurements, as well as very long baseline interferometry (VLBI) data, which together helped to improve the VTEC maps and derive improved ionospheric corrections. Alizadeh et al. (2011) investigated the global ionosphere modeling from GNSS, satellite altimetry, and F3/C data, and showed that the RMS of the combined GIMs decreased by approximately 0.1 TECU for an entire day. Zhang et al. (2013) proposed an inequality-constraint algorithm, which can eliminate unwanted negative VTEC values, and results were highly consistent with the final IGS products. Chen et al. (2015, 2017) constructed GIMs by integrating GNSS, satellite altimetry, radio occultation and DORIS data, while considering systematic biases among different data sets, and found that the accuracy of final the GIM improved significantly, especially over ocean areas. Sun et al. (2017) constructed near-real-time GIMs from GNSS measurements and F3/C GPS occultation data; results showed the F3/C TEC had an improvement on the GIM of approximately 15.5%, especially over ocean areas.

It now appears that the most effective way to improve the accuracy of the GIM is to increase the number of effective observations for ionospheric modeling. In our study, we will construct a global ionosphere model based on multisource

data, namely, multi-GNSS (GPS/GLONASS/BDS), satellite altimetry, and F3/C data. Specifically, the contribution of BDS observations to ionosphere modeling will be considered, especially in the Asia-Pacific region. The influence of satellite altimetry TEC data, which directly provide high-accuracy TEC and can compensate for insufficient GNSS coverage in ocean areas, and F3/C TEC data, which can obtain well-distributed ionospheric information over the globe, on GIMs will also be examined.

## Ionosphere observations acquisition from multisource data

Due to the dispersive characteristics of the ionosphere, the ionospheric TEC from multi-GNSS (GPS/GLONASS/BDS), satellite altimetry and F3/C data can be estimated from dual-frequency measurements.

### Ionospheric observables from multi-GNSS data

For multi-GNSS, by forming the geometry-free linear combination from the pseudorange and carrier observations, high-accuracy TEC can be obtained by leveling carrier to code algorithms. As shown below, we have expressions for the VTEC, STEC, and mapping function (MF):

$$\left. \begin{aligned} \text{VTEC} &= \text{MF} \cdot \text{STEC} \\ \text{STEC} &= \alpha_0 \cdot \left( \tilde{P}_{4,ij} + \text{DCB}_{\text{rcv},ij} + \text{DCB}_{ij}^{\text{sat}} \right) \\ \text{MF} &= \cos \left( \arcsin \left( \frac{R}{R + H_{\text{ion}}} \right) \sin(\alpha z) \right) \end{aligned} \right\} \quad (1)$$

where STEC is the line-of-sight (LOS) ionospheric TEC along the propagation path from satellite to receiver,  $\alpha_0 = f_i^2 f_j^2 / \left[ 40.3 (f_i^2 - f_j^2) \right]$ ,  $f_i$  and  $f_j$  are the GNSS signal frequencies,  $\tilde{P}_{4,ij}$  is the GNSS code-leveled carrier phase measurements of frequency  $f_i$  and  $f_j$ ;  $\text{DCB}_{\text{rcv},ij}$  and  $\text{DCB}_{ij}^{\text{sat}}$  are the differential code biases (DCB) of GNSS receivers and satellites, respectively; MF is the modified single-layer model (MSLM) MF, used for converting STEC to vertical TEC (VTEC),  $z$  is the satellite zenith angle at the station, and  $R$  is the earth's radius and it is set to 6371 km. Further,  $H_{\text{ion}} = 506.7$  km, and  $\alpha = 0.9782$ , which are consistent with the values used by the CODE analysis center. When all of the satellites in multi-GNSS systems are observed, the resulting normal equations matrix exhibit a rank deficiency since the DCB common to all satellites cannot be distinguished from the corresponding DCB common to all receivers. This rank deficiency is removed by imposing a

zero-mean condition on all satellites DCB estimates of each satellite system.

### Ionospheric observables from satellite altimetry

As to satellite altimetry, by measuring range on two different frequencies  $f_{Ku} = 13.575$  GHz and  $f_C = 5.3$  GHz, the TOPEX/JASON (T/J) altimeter can provide a direct VTEC over the oceans up to the T/J orbit altitude of 1336 km. If Ku band ionospheric range correction is calculated as presented by Brunini et al. (2005), the VTEC can be expressed as follows:

$$VTEC = -\frac{dR \cdot f_{Ku}^2}{40.3}, \tag{2}$$

where  $dR$  is the Ku band ionospheric range correction, and  $f_{Ku}$  is the Ku band frequency in GHz. Similar to the process suggested by Imel et al. (1994), the T/J VTEC used in our analysis is averaged over a 21-s smoothing window to reduce the inherent noise effects of the altimeter.

### Ionospheric observables from Formosat-3/COSMIC

For radio occultation data Formosat-3/COSMIC (F3/C), the ‘ionPrf’ products from CDAAC (<http://cdaac-www.cosmic.ucar.edu/cdaac/>) provide VTEC at the location of maximum electron density for each occultation event. They include ionospheric electron density from the ionospheric bottom up to the F3/C satellite orbit height, as well as the extrapolation from F3/C satellites to GPS satellites orbit height, namely,

$$VTEC = VTEC_0 + VTEC_1, \tag{3}$$

where  $VTEC_0$  is the VTEC under the F3/C satellite orbit, obtained through the application of an aided Abel inversion.  $VTEC_1$  is the plasmaspheric electron content above the F3/C satellite orbit (LEO to GPS altitude), which is calculated using extrapolation technique. For more details, see Liou et al. (2010).

Combining Eqs. (1), (2) and (3), the following formula can be obtained:

$$\left. \begin{aligned} L_{GNSS} &= MF \cdot \alpha_0 \cdot \left( \tilde{P}_{4,i,j} + DCB_{rcv,i,j} + DCB_{i,j}^{sat} \right) \\ L_{F3/C} &= VTEC_0 + VTEC_1 \\ L_{T/J} &= -\frac{dR \cdot f_{Ku}^2}{40.3} + Bias \end{aligned} \right\}, \tag{4}$$

where  $L_{GNSS}$ ,  $L_{F3/C}$  and  $L_{T/J}$  denote the VTEC derived from multi-GNSS, F3/C and satellite altimetry, respectively. Bias

denotes the systematic bias between GNSS and T/J VTEC measurements, which is modeled as unknown and estimated.

### Construction of global ionospheric maps

The VTEC obtained by different space-geodetic observation techniques is fitted by the spherical harmonic (SH) model with a degree and order of 15. The SH function can be expressed as (Schaer 1999):

$$GIM(\varphi, \lambda) = \sum_{n=0, m=0}^{n_{max}} \tilde{P}_{nm}(\sin \varphi) \cdot (\tilde{A}_{nm} \cos(m\lambda) + \tilde{B}_{nm} \sin(m\lambda)), \tag{5}$$

where  $\varphi$  and  $\lambda$  are the geomagnetic latitude and sun-fixed longitude of the IPP,  $GIM(\varphi, \lambda)$  is the VTEC at the IPP obtained from different observation techniques,  $n_{max}$  is the maximum degree of SH function, which is  $n_{max} = 15$  in this study.  $\tilde{P}_{nm}(\sin \varphi)$  denotes the normalized associated Legendre function with degree  $n$  and order  $m$ , and  $\tilde{A}_{nm}$  and  $\tilde{B}_{nm}$  are the SH coefficients to be estimated. In our data processing, the SH coefficients are estimated by least squares algorithms every 2 h on a global scale. To guarantee the continuity of the ionospheric TEC model between two neighboring sessions and days, we use piece-wise linear (PWL) functions to establish connections of VTEC from different sessions. Consequently, the observations from 22:00 UT of the previous day to 02:00 UT of the next day are used for estimating 15 sequential groups of SH coefficients in 1 day.

The normal equations are added for each type of observation:

$$\begin{aligned} N &= N_{GNSS} + N_{ALT} + N_{F3/C} \\ &= A_{GNSS}^T P A_{GNSS} + A_{ALT}^T P A_{ALT} + A_{F3/C}^T P A_{F3/C}, \end{aligned} \tag{6}$$

where  $N$  is the normal equation matrix,  $A$  is the design matrix, and  $P$  is the weight matrix shown in formula (7).

The temporal resolution of the model is 2 h, with a spatial resolution of  $2.5^\circ$  in latitude and  $5^\circ$  in longitude. The parameters to be solved by least-square adjustment are the spherical harmonic coefficients, receivers DCB and satellites DCB, as well as the systematic bias between GNSS and T/J VTEC measurements. To improve operation efficiency, the relevant normal equation stacking is adopted, and only nonzero elements are considered.

Within this study, due to different VTEC sources in the various ionospheric techniques, variance component estimation (VCE) is used to determine the final weight. In this procedure, an individual variance factor  $\sigma_0^2$ ,  $i = \{GNSS, ALT, F3/C\}$ , for each observation group is introduced to enable different weighting. The weight matrix is

$$P_{n \times n} = \begin{bmatrix} P_{GNSS} & 0 & 0 \\ 0 & P_{ALT} & 0 \\ 0 & 0 & P_{F3/C} \end{bmatrix} = \begin{bmatrix} \frac{\sigma_0^2}{\sigma_{GNSS}^2} P'_{GNSS} & 0 & 0 \\ 0 & \frac{\sigma_0^2}{\sigma_{ALT}^2} P'_{ALT} & 0 \\ 0 & 0 & \frac{\sigma_0^2}{\sigma_{F3/C}^2} P'_{F3/C} \end{bmatrix}, \tag{7}$$

where the square matrices  $P'_{GNSS}$ ,  $P'_{ALT}$  and  $P'_{F3/C}$  of size  $n_{GNSS}$ ,  $n_{ALT}$ , and  $n_{F3/C}$  are the original weight matrix from multi-GNSS, satellite altimetry and F3/C observations, respectively, and they are used for evaluating the initial precision of three ionospheric techniques;  $n = n_{GNSS} + n_{ALT} + n_{F3/C}$ ;  $n_{GNSS}$ ,  $n_{ALT}$  and  $n_{F3/C}$  represent the numbers of three types of observation. Since no realistic variance–covariance matrix for any of the data types is available, no weighting within the observation groups is done and no correlations are introduced.

In an iterative approach, each  $\sigma_{0_i}^2$  can be computed from the observation group residuals,

$$\hat{\sigma}_{0_i}^2 = \frac{V_i^T P_i V_i}{n_i - \text{tr}(N^{-1} N_i)}, \tag{8}$$

where  $V_i$  is the residual vector of size  $n_i$  for each group  $n_i$ ,  $i = \{GNSS, ALT, F3/C\}$ , and  $\hat{\sigma}_{0_i}^2$  is the a posteriori variances.

In accordance with Eq. (8), the weight matrix can be obtained according to the following formula:

$$\hat{P}_i = \frac{\text{const}}{\hat{\sigma}_{0_i}^2} P_i, \tag{9}$$

where const is a constant, which is usually selected from one of the  $\hat{\sigma}_{0_i}^2$ . The  $\hat{P}_i$  and  $P_i$  are the posterior weight matrix and the priori weight matrix of size  $n_i$ , respectively. The new weight matrix is then used to re-adjust the observation equations, and again the posterior variances and new weight matrix are calculated. These processes are repeated until the variances of unit weight of the various observations are equal, namely  $\hat{\sigma}_{0_{GNSS}}^2 = \hat{\sigma}_{0_{ALT}}^2 = \hat{\sigma}_{0_{F3/C}}^2$ . The detailed iterative calculation process of VCE can be found in Koch and Kusche (2002), Dettmering et al. (2011) and Chen et al. (2015).

### Validation and analysis

The GIMs using GPS/GLONASS, GPS/GLONASS/BDS, GPS/GLONASS plus satellite altimetry, GPS/GLONASS plus F3/C, and finally GPS/GLONASS/BDS plus satellite altimetry plus F3/C data are investigated. This study utilized the multisource data from 2014 to improve the accuracy of GIMs. GNSS data are selected from IGS tracking stations

and MGEX networks, with a sampling rate of 30 s and a cutoff elevation angle of 15°. The original sampling rate of JASON 2 is 1 s. To reduce the inherent noise effects of the altimeter, a 21-s smoothing window along the track is adopted. The F3/C VTEC below LEO satellites was directly measured, and the electron density above the LEO satellites is computed through extrapolation.

BIAS and RMS are used to qualify the GIM performances with respect to CODE-derived GIM, GPS-based TEC, and JASON TEC. The formula is as follows:

$$\left. \begin{aligned} \text{BIAS} &= \frac{1}{N} \sum_{i=1}^N (\text{VTEC}_{i,\text{GIM}} - \text{VTEC}_{i,\text{ref}}) \\ \text{RMS} &= \sqrt{\frac{1}{N} \sum_{i=1}^N (\text{VTEC}_{i,\text{GIM}} - \text{VTEC}_{i,\text{ref}})^2} \end{aligned} \right\}, \tag{10}$$

where  $\text{VTEC}_{i,\text{GIM}}$  is the TEC obtained from GIM and  $\text{VTEC}_{i,\text{ref}}$  is the reference TEC derived from CODE-derived GIM, GPS-based TEC, or JASON TEC;  $N$  is the total number of ionospheric VTEC from the GIM in 1 day.

### GIM: GPS/GLONASS data

The conventional GIM in this study, called SGG temporarily, is calculated from global GPS/GLONASS observations. To validate the SGG GIM products accuracy, we calculated the RMS and BIAS of different GIMs (JPL, UPC, ESA, and SGG) with respect to CODE. The number of IGS stations

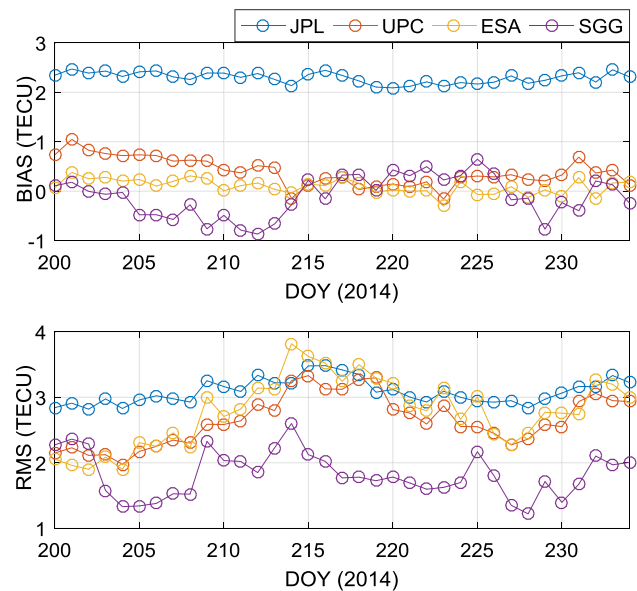


Fig. 1 BIAS and RMS of GIM for JPL, UPC, ESA and SGG with respect to CODE from DOY 200–234, 2014

used in SGG GIM computation is appropriately 220, which is a little lower than that used by CODE.

The statistical results with respect to CODE during DOY 200–234, 2014 are presented in Fig. 1. The figure shows that the BIAS for UPC, ESA, and SGG are within 1 TECU, which are in good agreement with each other, while the JPL BIAS with respect to CODE is nearly 2.2 TECU, and it seems that there is a systematic bias between JPL GIM and CODE GIM. The RMS of GIM for JPL, UPC, ESA, and SGG with respect to CODE are approximately (3–3.5, 2–3.6, 2–3.3, and 1.3–2.6) TECU, respectively; and it is shown that the ionospheric products of UPC, ESA and SGG agree well with CODE GIM,

The DCB is determined simultaneously with the calculation of GIM and is the most serious error that affects the estimated TEC accuracy. Therefore, the DCB can be used for evaluating the GIM accuracy. Here, the estimated GPS satellite P1–P2 DCBs are compared with the daily DCBs provided by CODE, JPL, UPC and ESA. The BIAS and RMS of the GPS satellites DCB with respect to CODE are shown in Fig. 2. It can be seen that the daily values for JPL, UPC and ESA are within 0.2 TECU, indicating a fairly good agreement, while the BIAS and RMS of SGG are mostly within 0.1 TECU. Therefore, it is obvious that the SGG DCB estimates are reliable compared with the products of CODE.

According to the performance of GIM-derived VTEC and P1–P2 DCB, it is clear that the SGG GIM has similar accuracy as the CODE GIM. Therefore, the SGG GIM is reliable. But considering the different data sources contributed to SGG and CODE, we compare our results with the SGG (GPS/GLONASS) GIM in the following sections.

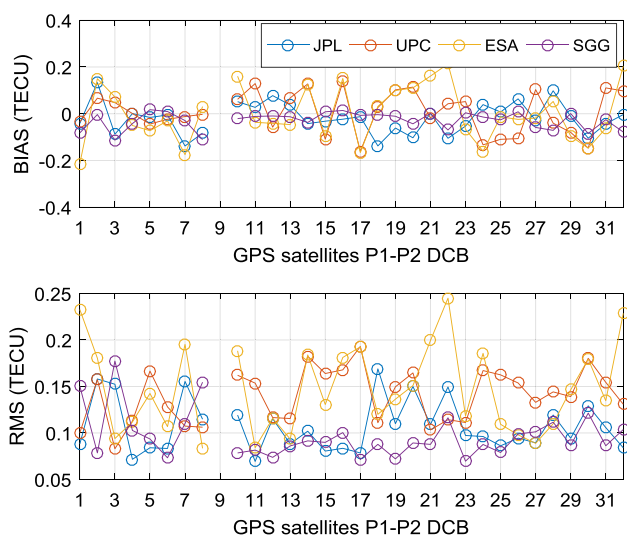


Fig. 2 BIAS and RMS of DCB (P1–P2) for JPL, UPC, ESA and SGG with respect to CODE from DOY 200 to DOY 234, 2014

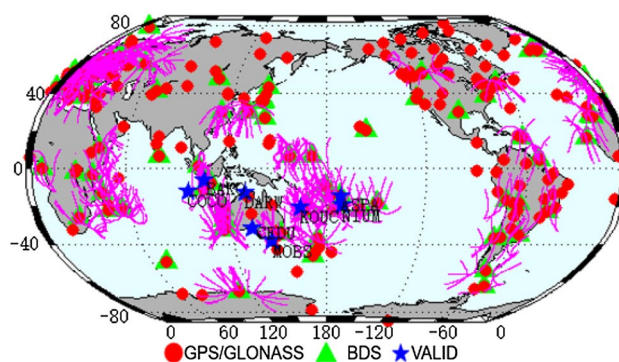


Fig. 3 GNSS sites’ distribution (DOY 200, 2014)

### GIM: GPS/GLONASS and BDS data

The GNSS site distribution is shown in Fig. 3. GPS/GLO-NASS indicates locations from IGS and MGEX networks, BDS indicates locations from MGEX, and VALID represents locations from IGS that do not participate in ionospheric modeling. The magenta curves represent BeiDou satellites IPPs. The GIM is generated using data from about 280 GNSS stations of the IGS and MGEX networks, while the DCBs of the GPS/GLONASS/BDS satellites and the receivers are estimated.

Figure 4 depicts the difference of GIMs computed with GPS/GLONASS/BDS and GPS/GLONASS at different periods. The VTEC changes by approximately ± 1 TECU after adding BeiDou data, and the most significant VTEC changes occur mainly over ocean areas. These changes are attributed to the fact that BDS observations increase IPP distributions.

To validate the improvement of GIM accuracy after adding BDS observations, the observations from VALID stations in Australia are used as external reference. It should be noted that these VALID stations are involved in the generation of CODE GIM, but not used for our GIM. The BIAS and RMS can be calculated by the following formulas (10) and (11):

$$\left. \begin{aligned} \text{VTEC}_{i,\text{ref}} &= \text{STEC}_{i,\text{GPS}} / \text{MF}_i \\ \text{STEC}_{i,\text{GPS}} &= \frac{f_1^2 f_2^2}{40.3(f_1^2 - f_2^2)} (P_{4,\text{sm}} - c\text{DCB}_{\text{GPS\_rcv}} - c\text{DCB}_{\text{GPS\_sat}}) \end{aligned} \right\} \quad (11)$$

where  $\text{STEC}_{i,\text{GPS}}$  is the  $i$ th STEC obtained from GPS data in each VALID station;  $f_1$  and  $f_2$  are the frequencies;  $\text{DCB}_{\text{GPS\_rcv}}$  and  $\text{DCB}_{\text{GPS\_sat}}$  are the GPS receiver and satellite P1–P2 DCBs from CODE, respectively;  $P_{4,\text{sm}}$  is the observation from the phase-smoothing pseudorange method;  $c$  is the speed of light in a vacuum;  $\text{MF}_i$  is the MF used in Eq. (1). To reduce the error from the MF and multipath, the elevation cutoff is selected as 30°.

**Fig. 4** GIM difference between those modeled with GPS/GLO-NASS/BDS and those modeled with GPS/GLONASS (DOY 200, 2014)

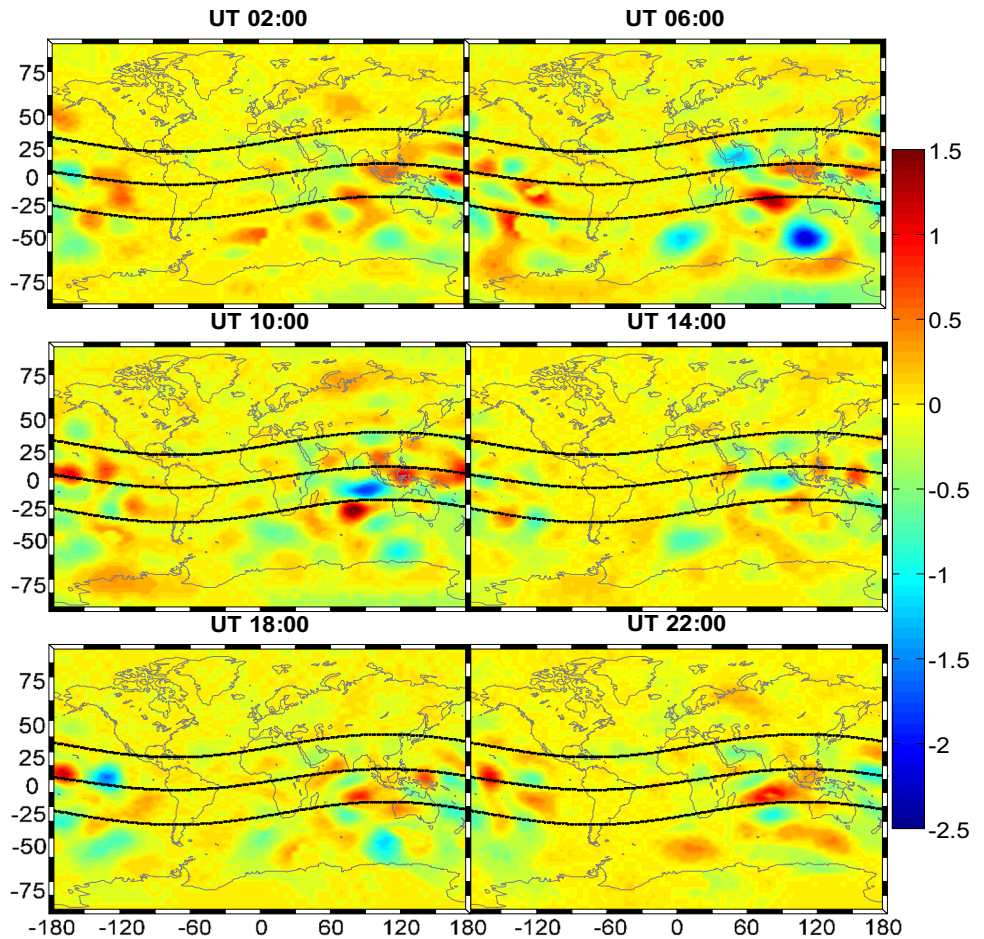


**Table 1** RMS and BIAS of the calculated GIM, with and without BDS data, validated by eight IGS stations

VALID stations	RMS (no BDS)	RMS (with BDS)	BIAS (no BDS)	BIAS (with BDS)
DARW	2.1941	2.0717	0.6958	0.7401
COCO	3.5105	3.0422	- 2.8668	- 2.5183
CEDU	1.4708	1.4358	- 0.3499	- 0.2116
KOUC	1.9625	1.9150	- 0.2455	0.2958
MOBS	1.6924	1.6624	- 0.2452	- 0.0305
BAKO	3.4334	3.2302	- 2.5715	- 2.4407
NIUM	1.7396	1.7177	0.6166	0.696
ASPA	1.9340	1.7288	- 0.1092	- 0.0935
Mean value	2.2422	2.1005	- 0.6345	- 0.4454

The validation of the calculated GIM using GPS-based ionospheric TEC from eight VALID stations are shown in Table 1. It can be observed that the calculated GIM with BDS data has better performance than the GIM without BDS data: the mean BIAS improves from -0.63 to -0.44 TECU, and the mean RMS decreases from 2.24 to 2.10 TECU. This is due to the contribution of BDS data over this area on the calculated GIM. The improvement is small, which may be attributed to limited BDS observations.

As a by-product of TEC calculation, the DCBs of satellites and receivers can reflect the accuracy and reliability of the GIM to a certain extent. Currently, multi-system DCB products are released by the Chinese Academy of Sciences (CAS) and the German Aerospace Center (DLR). In this study, the BDS DCB products published by CAS/DLR are regarded as a reference, and we take BDS satellite DCB C2I-C7I as an example, here C2I and C7I are two BDS code observation types. Figure 5 shows the satellites' DCB comparison between our results (WHU) and CAS/DLR products.

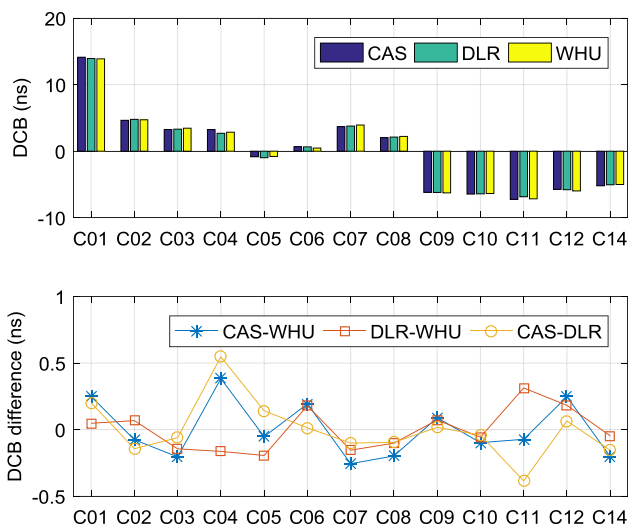


**Fig. 5** BDS satellite DCB (C21–C71) results from CAS, DLR, and WHU, as well as differences among them (DOY 200, 2014)

In this case, the WHU DCBs are in a rather good agreement with the CAS and DLR products, and the difference is mostly within 0.2 ns. This indicates that the DCB products of WHU and CAS/DLR achieve the same level of accuracy. From Figs. 3, 4 and 5, we can conclude that BDS observations increase the spatial coverage of IPPs, especially over

Australia, East Asia, and Europe. Thus, our results show that the contribution of BDS observations on model RMS is evident in the region of Australia.

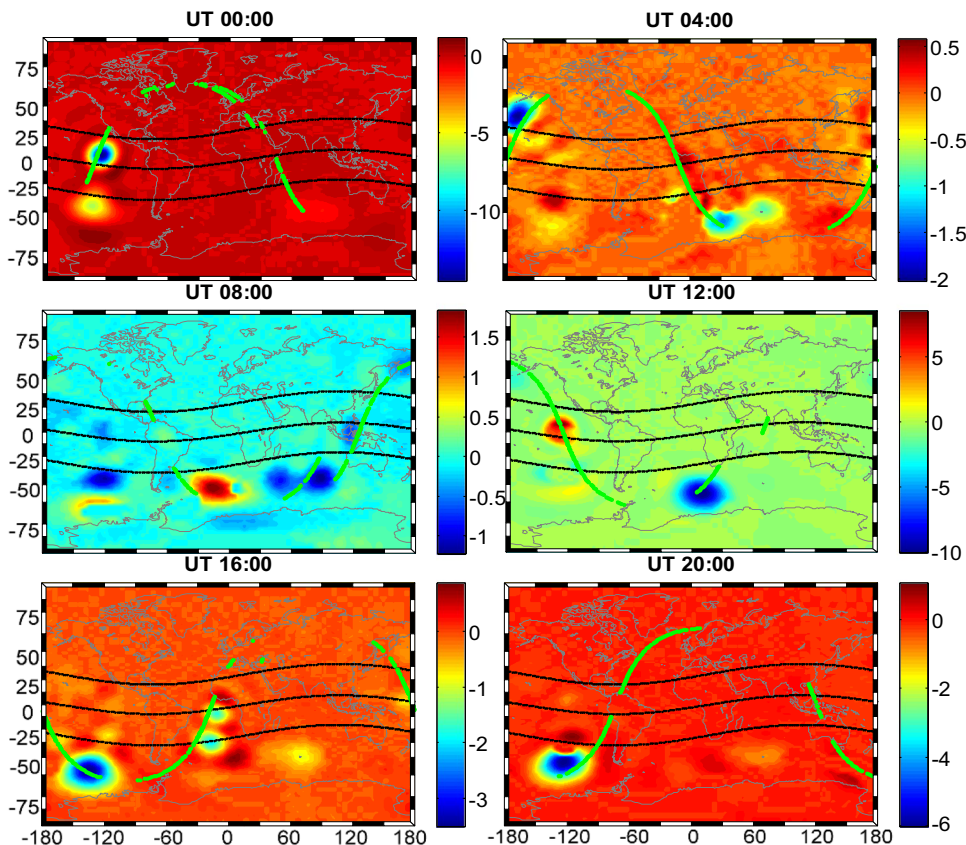
**GIM: GPS/GLONASS and altimetry data**

As shown in Fig. 6, the VTEC changes greatly over ocean areas and regions that lack IGS stations. The most significant differences are exactly located at areas along JASON 2 footprints, and the maximum difference 15 TECU, whereas there is little VTEC change for densely GNSS monitored areas with minor difference within 1 TECU.

To further illustrate the effectiveness of combining GPS/GLONASS data and JASON 2 data for ionospheric modeling, some measured VTEC data of JASON 2 not involved in modeling are selected as reference values to validate the external accuracy of GIM performance. During calculation, it should be noted that VTEC from GIM is interpolated to the altimetry satellite footprint location through a bivariate spatial interpolation scheme and linear time interpolation between two consecutive GIMs.

The statistical results (residuals, BIAS and RMS) of two GIMs with respect to the reference values are shown in Fig. 7. It can be seen that by combining JASON 2 altimetry satellite data, the residual distribution is much more

**Fig. 6** GIM difference between those modeled with GPS/GLO-NASS data and those modeled with GPS/GLONASS and JASON 2 data (DOY 200, 2014)



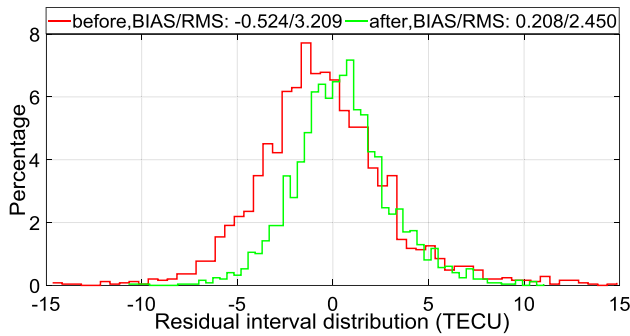


**Fig. 7** Residual distribution for GIM with respect to JASON 2 VTEC (not used for the generation of GIM), DOY 200, 2014. GPS/GLO-NASS (red) and GPS/GLONASS and JASON 2 (green)

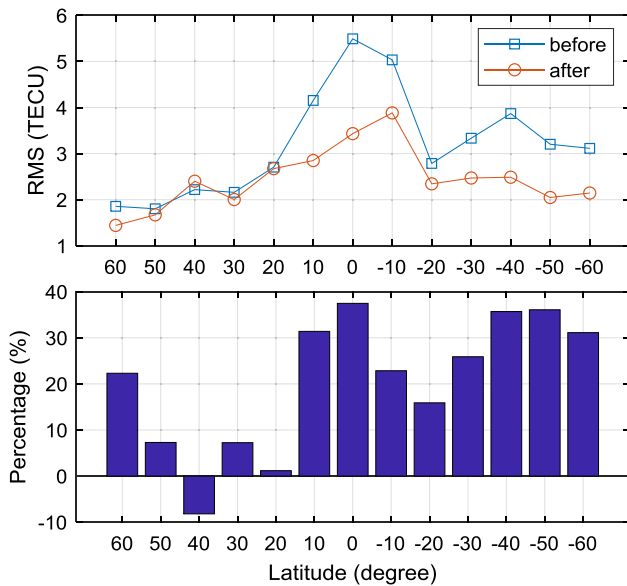


**Fig. 8** RMS statistics over different latitudes for GIM (GPS/GLONASS) and GIM (GPS/GLONASS and JASON 2) compared to JASON 2 VTEC (not involved in modeling), DOY 200, 2014

concentrated; The BIAS reduces from  $-0.52$  to  $0.21$  TECU, and RMS reduces from  $3.21$  to  $2.45$  TECU.

Figure 8 shows the RMS statistics of each latitude zone with respect to some extra JASON 2 observations. After the introduction of JASON 2 data, the RMS has been reduced at various latitudes, and the entire RMS improvement is more than 10%. The RMS improvement is especially obvious in mid-high latitudes of the southern hemisphere and in the equatorial region, where the RMS is generally improved by 20–35%. It should be pointed out that these statistical results only denote the improvement of the GIM over the ocean and not over the land. The reason is that there are only a few GNSS stations in these areas but abundant JASON 2 data coverage. The latter, without any doubt, improves the GIM accuracy in these areas. Furthermore, the ionospheric

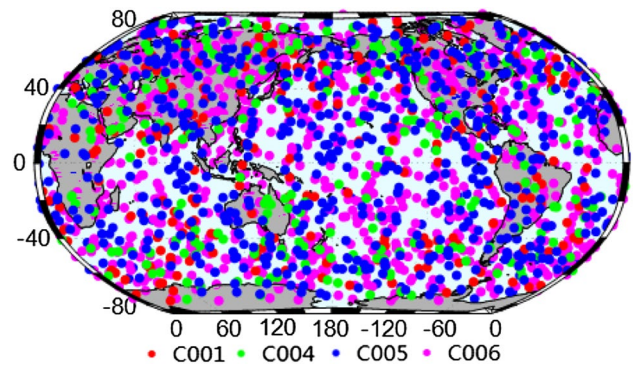


**Fig. 9** Distribution of F3/C ionospheric occultation events (DOY 200, 2014)

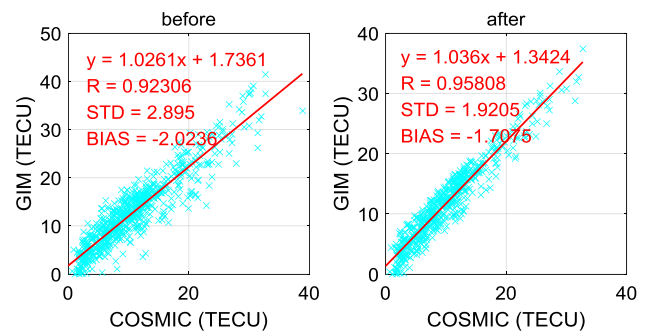


**Fig. 10** Influence on modeling after adding F3/C data (DOY 200, 2014)

mapping function error at the equator for conventional GNSS-based modeling is high, but the mapping function and its associated error are perfectly avoided in deriving JASON 2 VTEC observations.

### GIM: GPS/GLONASS and F3/C data

Figure 9 shows the global distribution of F3/C radio occultation data. There are approximately 700 occultation events for all satellites (C001, C004, C005 and C006) in DOY 200, 2014, and they are evenly distributed around the globe.

Figure 10 shows the impact of adding F3/C data on the modeling results. Compared to the GIM modeled with GPS/GLONASS data, adding F3/C VTEC data improves the GIM accuracy: The correlation coefficient between GIM and F3/C increases from 0.92 to 0.96, while standard deviation and BIAS show minor improvements, i.e., standard deviation reduces from 2.89 to 1.92 TECU, and BIAS decreases from  $-2.02$  to  $-1.71$  TECU. The accuracy enhancement is not that significant, mainly because, even though the F3/C occultation events evenly distributed around the globe, the F3/C data available are much less than that of GNSS data.

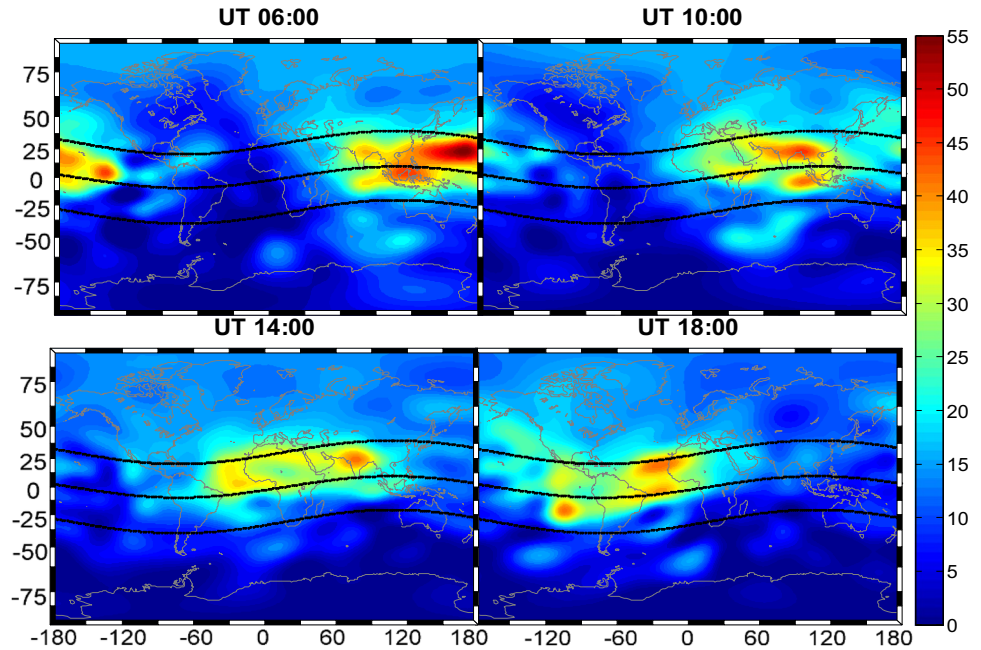
Hence, F3/C has some contribution to GIM, but it is not that significant. With the future development and upgrading of COSMIC-2, much more contribution of COSMIC data to GIMs can be expected.

### GIM: GPS/GLONASS/BDS, JASON 2, and F3/C data

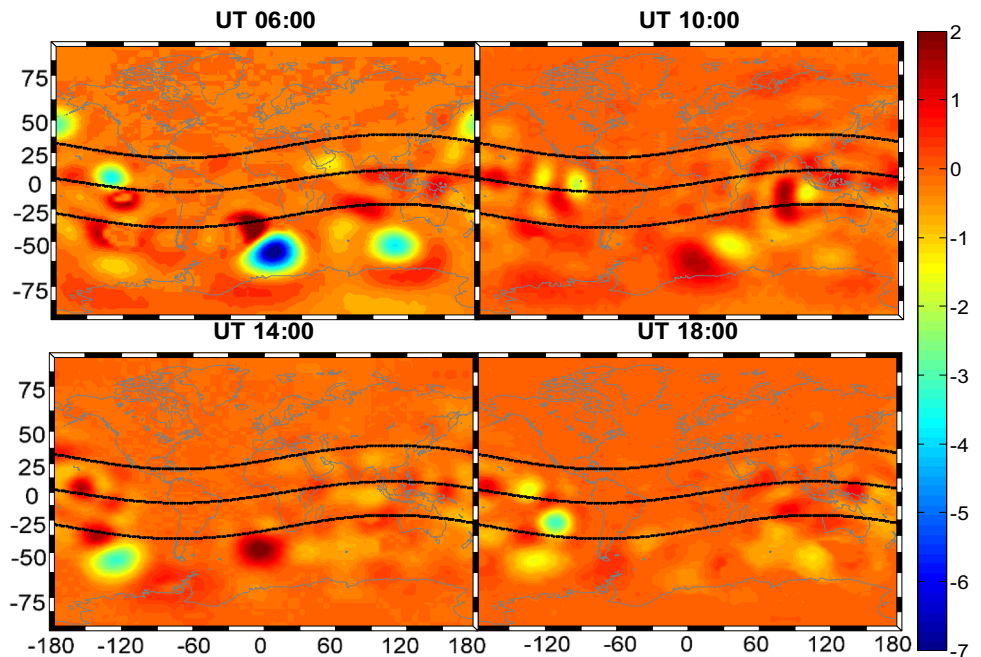
The GIMs based on multi-GNSS, JASON 2, and F3/C data are shown in Fig. 11. The equatorial anomaly area can be clearly seen at low latitudes, which is consistent with

ionospheric diurnal variation. Figure 12 illustrates the difference between GIM including GPS/GLONASS-only data and that including multisource data. As expected, the difference, approximately  $\pm 2$  TECU, in the northern hemisphere is a result of a large number of GNSS receivers, and the contribution of BDS, JASON 2, and F3/C. It should be noted that the VTEC difference in the southern hemisphere is particularly obvious and can reach more than 4 TECU. These larger discrepancies are mainly caused by the contribution of JASON 2 data, which is widely distributed over

**Fig. 11** GIMs calculated by multi-GNSS, JASON 2, and F3/C data (DOY 200, 2014)



**Fig. 12** Difference maps between those modeled with GPS/GLONASS data and those modeled with GPS/GLONASS/BDS, JASON 2 and F3/C data (DOY 200 2014)



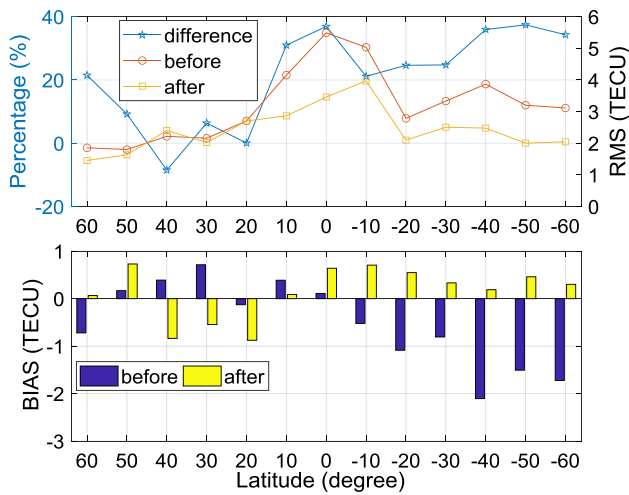


**Fig. 13** RMS (top) and BIAS (bottom) statistics over different latitude bands for GIM (GPS/GLONASS) and GIM (GPS/GLONASS/BDS, F3/C, and JASON 2) compared to JASON 2 VTEC (not involved in modeling), DOY 200, 2014

oceans of the southern hemisphere. In addition, the conventional GIMs based on global basis expansions, such as the SH expansion, are more affected by the unbalanced amount of GNSS observations, although much less at the southern hemisphere than the combined GIM models. The uneven IPPs distribution in space distorts the inverted SH coefficients and thus is expected to affect the conventional GIM product performance.

To further validate the GIM improvement based on multi-source data, some extra JASON 2 VTEC values are regarded as reference values. Then, the RMS and BIAS of two kinds of GIMs (before: GPS/GLONASS; after: GPS/GLONASS/BDS, JASON 2, and F3/C) are calculated for an external assessment of performance. The RMS and BIAS of the two GIMs in different latitude bands are shown in Fig. 13. The RMS decreases from [2, 5] to [2, 3] TECU, and the RMS improvement percentage is 20–35% in mid-high latitudes of the southern hemisphere and in the equatorial region. The BIAS decreases from [−3, 1] to [−1, 1] TECU, with evident BIAS improvement in the middle and high latitude regions of the southern hemisphere.

Figure 14 shows the BIAS and RMS of the ionospheric VTEC for the CODE GIM, the SGG GIM and the combined GIM, where extra JASON 2 VTEC from DOY 200 to 235, 2014, is considered as a reference value. Compared with the VTEC of the JASON 2 satellite footprint, the VTEC from CODE and SGG has similar accuracy, which agrees well with the aforementioned validation in Fig. 1. In terms of RMS and BIAS, the combined GIM from multisource data has better performance than that from SGG and CODE. The SGG GIMs and CODE GIMs are more affected by the unbalanced amount of GNSS observations, but much less at

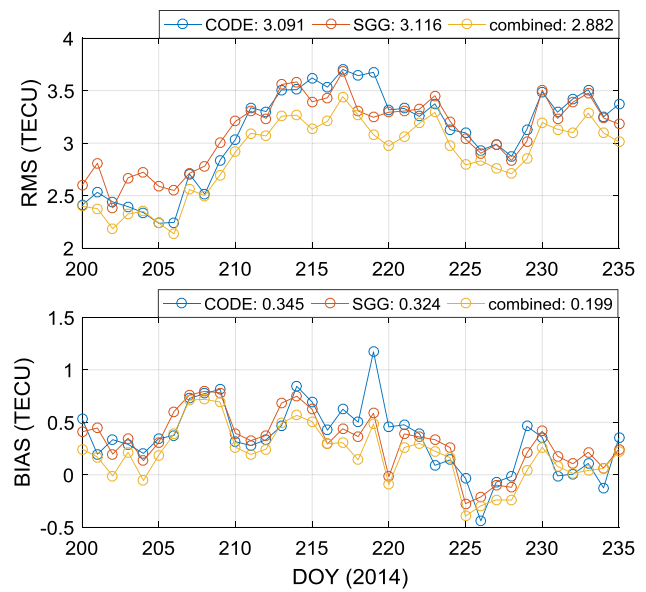


**Fig. 14** Statistical results of the CODE/SGG/combined GIM validated by extra JASON 2 VTEC from DOY 200–235, 2014

the southern hemisphere than the combined GIM models. For example, the uneven IPP distribution in space distorts the inverted SH coefficients and thus is expected to affect the conventional GIM products performance. However, our combined GIM has the big advantage of improving global ionospheric modeling performance. Because the satellite altimetry and F3/C VTEC data can compensate the insufficient GNSS coverage in ocean areas, which improves GIM accuracy in these areas.

### Conclusions

The combined GIM constructed from multisource data (GPS/GLONASS/BDS, JASON 2, and F3/C data) is fitted by the SH expansion with a degree and order of 15. It is shown that global ionospheric modeling based on multisource data can improve the GIM accuracy and reliability globally, especially over ocean areas. The VTEC difference between conventional GIM (from GPS/GLONASS data) and combined GIM (derived from multisource data) varies around the globe. The difference is small and approximately  $\pm 2$  TECU in the northern hemisphere, whereas the difference is much larger in the southern hemisphere. In different latitude bands, the RMS of the combined GIM decreases from [2, 5] to [2, 3] TECU, and the BIAS decreases from [−3, 1] to [−1, 1] TECU. From the statistical results of the CODE/SGG/combined GIM, validated by extra JASON 2 VTEC over long periods, it is obvious that the combined GIM from multisource data has a much better performance.

Specifically, BDS observations help to increase the spatial coverage of the IPPs, especially in the region of Australia. Compared with GPS-based ionospheric TEC, our calculated GIM with BDS data has better performance than that without BDS data: the mean BIAS improves from  $-0.63$  to  $-0.44$  TECU, and the mean RMS decreases from 2.24 to 2.10 TECU. On the other hand, the BDS DCB is the by-product of TEC calculation and must be estimated accurately for high-precision ionospheric modeling. Our results show that the BDS DCBs (C2I–C7I) are in a good agreement with CAS/ DLR products. By combining JASON 2 and GPS/GLONASS data, the residual distribution is much more concentrated, and the VTEC accuracy improves significantly over ocean areas with JASON 2 data footprint coverage. The RMS is generally improved by 20–35% in mid-high latitudes of the southern hemisphere and in the equatorial region. This is due to there being few GNSS stations in these areas but abundant JASON 2 data coverage, which undoubtedly improves GIM accuracy in these areas. F3/C VTEC results into minor improvements on the GIM; the correlation coefficient between two GIMs and F3/C increases from 0.92 to 0.96, the standard deviation reduces from 2.89 to 1.92 TECU, and the BIAS decreases from  $-2.02$  to  $-1.71$  TECU.

With the development of multi-GNSS (especially BDS and Galileo), satellite altimetry and COSMIC-2, as well as other ionospheric sounding techniques, much higher-precision GIMs are expected in the future. On the other hand, considering the limitation of the current SH order and degree, we will focus on increasing higher SH degree and order to reduce GIM errors in our further study.

**Acknowledgements** This work was supported by the National Key Research and Development Program of China (No. 2016YFB0501803), the National Natural Science Foundation of China (No. 41574028), and the Natural Science Foundation for Distinguished Young Scholars of Hubei Province of China (No. 2015CFA036). The authors gratefully acknowledge the CDDIS for GNSS observations, NOAA for satellite altimetry data, and CDAAC for F3/C “ionPrf” products.

## References

- Alizadeh MM, Schuh H, Todorova S, Schmidt M (2011) Global ionosphere maps of VTEC from GNSS, satellite altimetry, and Formosat-3/COSMIC data. *J Geodesy* 85(12):975–987
- Brunini C, Meza A, Bosch W (2005) Temporal and spatial variability of the bias between TOPEX- and GPS-derived total electron content. *J Geodesy* 79(4–5):175–188
- Chen P, Yao W, Zhu X (2015) Combination of ground-and space-based data to establish a global ionospheric grid model. *IEEE Trans Geosci Remote Sens* 53(2):1073–1081
- Chen P, Yao Y, Yao W (2017) Global ionosphere maps based on GNSS, satellite altimetry, radio occultation and DORIS. *GPS Solut* 21(2):639–650
- Dettmering D, Schmidt M, Heinkelmann R, Seitz M (2011) Combination of different space-geodetic observations for regional ionosphere modeling. *J Geod* 85(12):989–998
- Feltens J (2007) Development of a new three-dimensional mathematical ionosphere model at European space agency/European space operations centre. *Space Weather* 5(12):1–17
- Hernández-Pajares M, Juan JM, Sanz J (1999) New approaches in global ionospheric determination using ground GPS data. *J Atmos Solar-Terr Phys* 61(16):1237–1247
- Hernández-Pajares M, Juan JM, Sanz J, Orus R, Garcia-Rigo A, Feltens J, Komjathy A, Schaer SC, Krankowski A (2009) The IGS VTEC maps: a reliable source of ionospheric information since 1998. *J Geodesy* 83(3):263–275
- Imel DA (1994) Evaluation of the TOPEX/POSEIDON dual-frequency ionosphere correction. *J Geophys Res: Oceans* 99(C12):24895–24906
- Koch KR, Kusche J (2002) Regularization of geopotential determination from satellite data by variance components. *J Geodesy* 76(5):259–268
- Li Z, Yuan Y, Li H, Ou J, Huo X (2012) Two-step method for the determination of the differential code biases of COMPASS satellites. *J Geodesy* 86(11):1059–1076
- Li Z, Yuan Y, Wang N, Hernandez-Pajares M, Huo X (2015) SHPTS: towards a new method for generating precise global ionospheric TEC map based on spherical harmonic and generalized trigonometric series functions. *J Geodesy* 89(4):331–345
- Liou YA, Pavelyev AG, Matugov SS, Yakovlev OI, Wickert J (2010) Radio occultation method for remote sensing of the atmosphere and ionosphere. I-Tech Education and Publishing KG, Croatia, p 176 (ISBN 978-953-7619-60-2)
- Mannucci AJ, Wilson BD, Yuan DN, Ho CH, Lindqwister UJ, Runge TF (1998) A global mapping technique for GPS-derived ionospheric total electron content measurements. *Radio Sci* 33(3):565–582
- Orús R, Hernández-Pajares M, Juan JM, Sanz J, Garcia-Fernandez M (2003) Validation of the GPS TEC maps with TOPEX data. *Adv Space Res* 31(3):621–627
- Roma-Dollase D et al (2017) Consistency of seven different GNSS global ionospheric mapping techniques during one solar cycle. *J Geodesy* 92(6):691–706
- Schaer S (1999) Mapping and predicting the earths ionosphere using the global positioning system. Ph.D. thesis, Ph.D. dissertation. University of Bern, Bern
- Sun YY, Liu JY, Tsai HF, Krankowski A (2017) Global ionosphere map constructed by using total electron content from ground-based GNSS receiver and FORMOSAT-3/COSMIC GPS occultation experiment. *GPS Solut* 21(4):1583–1591
- Tang W, Jin L, Xu K (2014) Performance analysis of ionosphere monitoring with BeiDou CORS observational data. *J Navig* 67(3):511–522
- Xue J, Song S, Zhu W (2016) Estimation of differential code biases for Beidou navigation system using multi-GNSS observations: how stable are the differential satellite and receiver code biases? *J Geodesy* 90(4):309–321
- Yuan Y, Tscherning CC, Knudsen P, Xu G, Ou J (2008) The ionospheric eclipse factor method (IEFM) and its application to determining the ionospheric delay for GPS. *J Geodesy* 82(1):1–8
- Zhang H, Xu P, Han W, Ge M, Shi C (2013) Eliminating negative VTEC in global ionosphere maps using inequality-constrained least squares. *Adv Space Res* 51(6):988–1000
- Zhang R, Song WW, Yao YB, Shi C, Lou YD, Yi WT (2015) Modeling regional ionospheric delay with ground-based BeiDou and GPS observations in China. *GPS Solut* 19(4):649–658



**Yibin Yao** is currently a Professor at School of Geodesy and Geomatics, Wuhan University, China. He obtained his Ph.D. degree in Geodesy and Surveying Engineering from the Wuhan University in 2004. His current research interests include GNSS ionospheric/atmospheric/meteorological studies and high-precision GNSS data processing.



**Jian Kong** is a postdoctoral researcher at the Chinese Antarctic Center of Surveying and Mapping, Wuhan University, Wuhan, China. He obtained his Ph.D. degree in 2014. His current researches are focused on ionosphere disturbances in severe space weather events, i.e., earthquakes and typhoons.



**Lei Liu** is currently a Ph.D. student at Wuhan University, China. His research interests include ground-based and space-based ionosphere/plasmasphere monitoring, and ionospheric disturbances related to magnetic storms.



**Changzhi Zhai** is currently a Ph.D. student at Wuhan University, China. He received his master degree in Geodesy and Geomatics in 2017 at Wuhan University. His current research focuses mainly involve GNSS ionosphere disturbances related to earthquakes.